

# Asteroseismic modelling of the solar-type subgiant star $\beta$ Hydri

I. M. Brandão<sup>1,2</sup>, G. Doğan<sup>3</sup>, J. Christensen-Dalsgaard<sup>3</sup>, M. S. Cunha<sup>1</sup>, T. R. Bedding<sup>4</sup>,  
T. S. Metcalfe<sup>5</sup>, H. Kjeldsen<sup>3</sup>, H. Bruntt<sup>3,6</sup>, and T. Arentoft<sup>3</sup>

<sup>1</sup> Centro de Astrofísica da Universidade do Porto, Rua das Estrelas, 4150-762 Porto, Portugal  
e-mail: isa@astro.up.pt

<sup>2</sup> Departamento de Física e Astronomia, Faculdade de Ciências da Universidade do Porto, Portugal

<sup>3</sup> Department of Physics and Astronomy, Aarhus University, 8000 Aarhus C, Denmark

<sup>4</sup> Sydney Institute for Astronomy (SIFA), School of Physics, University of Sydney, Australia

<sup>5</sup> High Altitude Observatory and Technology Development Division, NCAR, Boulder, Colorado, USA

<sup>6</sup> Observatoire de Paris, LESIA, 5 place Jules Janssen, 92195 Meudon Cedex, France

Received 9 July 2010 / Accepted 22 November 2010

## ABSTRACT

**Context.** Comparing models and data of pulsating stars is a powerful way to understand the stellar structure better. Moreover, such comparisons are necessary to make improvements to the physics of the stellar models, since they do not yet perfectly represent either the interior or especially the surface layers of stars. Because  $\beta$  Hydri is an evolved solar-type pulsator with mixed modes in its frequency spectrum, it is very interesting for asteroseismic studies.

**Aims.** The goal of the present work is to search for a representative model of the solar-type star  $\beta$  Hydri, based on up-to-date non-seismic and seismic data.

**Methods.** We present a revised list of frequencies for 33 modes, which we produced by analysing the power spectrum of the published observations again using a new weighting scheme that minimises the daily sidelobes. We ran several grids of evolutionary models with different input parameters and different physics, using the stellar evolutionary code ASTEC. For the models that are inside the observed error box of  $\beta$  Hydri, we computed their frequencies with the pulsation code ADIPLS. We used two approaches to find the model that oscillates with the frequencies that are closest to the observed frequencies of  $\beta$  Hydri: (i) we assume that the best model is the one that reproduces the star's interior based on the radial oscillation frequencies alone, to which we have applied the correction for the near-surface effects; (ii) we assume that the best model is the one that produces the lowest value of the chi-square ( $\chi^2$ ), i.e. that minimises the difference between the observed frequencies of all available modes and the model predictions, after all model frequencies are corrected for near-surface effects.

**Results.** We show that after applying a correction for near-surface effects to the frequencies of the best models, we can reproduce the observed modes well, including those that have mixed mode character. The model that gives the lowest value of the  $\chi^2$  is a post-main-sequence model with a mass of  $1.04 M_{\odot}$  and a metallicity slightly lower than that of the Sun. Our results underscore the importance of having individual frequencies to constrain the properties of the stellar model.

**Key words.** asteroseismology – stars: solar-type – stars: individual:  $\beta$  Hydri

## 1. Introduction

The source  $\beta$  Hydri ( $\beta$  Hyi, HD 2151, HR 98, HIP 2021) is a single, bright subgiant star ( $m_V = 2.80$ ) that is clearly visible to the naked eye about  $12^\circ$  from the South Pole. It is the closest subgiant star, with a spectral and luminosity type between G2 IV (Hoffleit & Warren 1995; Evans et al. 1957) and G0 V (Gray et al. 2006), and it is one of the oldest stars in the solar Galactic neighbourhood. It is frequently regarded as representing the future of the Sun (Dravins et al. 1993c,b,a), making it a particularly interesting object of study.

Improvements to the fundamental parameters of  $\beta$  Hyi have been presented in a number of recent papers. Recent interferometric measurements of  $\beta$  Hyi have yielded an accurate (0.8%) angular diameter for this star (North et al. 2007). Also, the *Hipparcos* parallax of  $\beta$  Hyi has been improved from an uncertainty of 0.4% (Perryman & ESA 1997) to 0.08% (van Leeuwen 2007). The combination of these two values gives a direct measure of  $\beta$  Hyi's radius with high accuracy. Moreover, since the bolometric flux of this star is known

(Blackwell & Lynas-Gray 1998), its position in the Hertzsprung-Russell (HR) diagram is, in principle, well-constrained.

Frandsen (1987) and Edmonds & Cram (1995) made unsuccessful attempts to detect stellar oscillations in  $\beta$  Hyi, placing upper limits on the p-mode amplitudes. Bedding et al. (2001) and Carrier et al. (2001) finally confirmed the presence of solar-like oscillations in  $\beta$  Hyi and estimated the large frequency separation  $\Delta\nu$  to be about  $55 \mu\text{Hz}$ , but were unable to identify individual mode frequencies. Subsequently, Bedding et al. (2007) observed  $\beta$  Hyi during more than a week with the high-precision spectrographs HARPS and UCLES. Besides confirming the oscillations detected in their previous observations in 2000, they were able to identify 28 oscillation modes that included some mixed modes of spherical degree  $l = 1$ . Mixed modes occur in stars that have left the main-sequence stage of their evolution (e.g. Osaki 1975; Aizenman et al. 1977), and they provide useful information about the core. The presence of mixed modes, together with the availability of very precise non-seismic and seismic data for  $\beta$  Hyi, places the star in a privileged position for asteroseismic studies (e.g. Cunha et al. 2007).

Theoretical models of  $\beta$  Hvi based on its seismic and non-seismic data have been published by [Fernandes & Monteiro \(2003\)](#), [Di Mauro et al. \(2003\)](#), and [Doğan et al. \(2009\)](#). [Fernandes & Monteiro \(2003\)](#) examined the position of  $\beta$  Hvi in the HR diagram by first considering the non-seismic data of the star. In order to estimate the mass of  $\beta$  Hvi, they used available seismic data, namely the large frequency separation, to remove partially the helium-content vs. mass degeneracy that exists when only non-seismic observational constraints are used. They also emphasized the usefulness of individual frequencies to constrain the age of  $\beta$  Hvi due to the presence of mixed modes in its observed oscillation spectrum. [Di Mauro et al. \(2003\)](#) computed models of  $\beta$  Hvi, also based on its global parameters. They used the oscillation frequencies of  $\beta$  Hvi to compare with the model frequencies. Their theoretical models reproduced the observed oscillation spectrum of  $\beta$  Hvi well, as well as the observed large and small frequency separations, after they applied an ad-hoc shift to the computed frequencies. In fact, when comparing the computed and the observed frequencies, one should bear in mind that there may be an offset between them. This offset is well known from helioseismology and is also present when comparing the observed and computed frequencies for other stars. It arises from improper modelling of the surface layers of stars. [Kjeldsen et al. \(2008\)](#) used solar data to derive an empirical correction for the near-surface offset which can be applied to stars other than the Sun. In our work, we apply this empirical correction to the model frequencies of  $\beta$  Hvi before comparing to the observed ones. We extend the analysis of [Doğan et al. \(2009\)](#), and also present a detailed discussion on the application of the near-surface correction.

## 2. Observational constraints

### 2.1. Non-seismic data

The most recent determination of the radius of  $\beta$  Hvi is given by [Kjeldsen et al. \(2008\)](#). The radius was obtained by combining the interferometric angular diameter of the star,  $\theta = 2.257 \pm 0.019$  mas ([North et al. 2007](#)), with the revised *Hipparcos* parallax,  $\pi_p = 134.07 \pm 0.11$  mas ([van Leeuwen 2007](#)).

The luminosity,  $L$ , of a star can be obtained through the relation,

$$L = 4\pi F_{\text{bol}} C^2 / \pi_p^2, \quad (1)$$

where  $F_{\text{bol}}$  is the bolometric flux and  $C$  is the conversion factor from parsecs to metres. To compute the luminosity of  $\beta$  Hvi we used the same value for the bolometric flux as [North et al. \(2007\)](#),  $F_{\text{bol}} = (2.019 \pm 0.05) \times 10^9 \text{ W m}^{-2}$  ([Blackwell & Lynas-Gray 1998](#), the uncertainty on  $F_{\text{bol}}$  is from [di Benedetto 1998](#)) and the revised *Hipparcos* parallax ([van Leeuwen 2007](#)). Adopting  $L_{\odot} = 3.842 \times 10^{26} \text{ W}$  with an uncertainty of 0.4% ([Bahcall et al. 2001](#)), we found  $L = 3.494 \pm 0.087 L_{\odot}$  for  $\beta$  Hvi.

A number of determinations of the effective temperature ( $T_{\text{eff}}$ ) of  $\beta$  Hvi can be found in the literature (e.g. [Favata et al. 1997](#); [Blackwell & Lynas-Gray 1998](#); [di Benedetto 1998](#); [Santos et al. 2005](#); [da Silva et al. 2006](#); [Biazzo et al. 2007](#); [Bruntt et al. 2010](#)). We adopted the value of [North et al. \(2007\)](#), which is derived from the direct measurement of the angular diameter.

The most recent value for the metallicity of  $\beta$  Hvi is given by [Bruntt et al. \(2010\)](#),  $[\text{Fe}/\text{H}] = -0.10 \pm 0.07$ . This value is in agreement with the one found by [Santos et al. \(2005\)](#),  $[\text{Fe}/\text{H}] = -0.08 \pm 0.04$  and with the one adopted by [Fernandes & Monteiro \(2003\)](#),  $[\text{Fe}/\text{H}] = -0.12 \pm 0.047$ . In our analysis we adopted the metallicity from [Bruntt et al. \(2010\)](#).

We calculated the mass fraction of metals,  $Z$ , from the metallicity using the following approximation, valid for Population I stars which do not present the  $\alpha$ -elements enrichment seen in metal deficient stars ([Wheeler et al. 1989](#)):

$$\begin{aligned} [\text{Fe}/\text{H}]_s &\equiv \log\left(\frac{Z_{\text{Fe}}}{Z}\right)_s + \log\left(\frac{Z}{X}\right)_s - \log\left(\frac{Z_{\text{Fe}}}{Z}\right)_{\odot} - \log\left(\frac{Z}{X}\right)_{\odot} \\ &= \log\left(\frac{Z}{X}\right)_s - \log\left(\frac{Z}{X}\right)_{\odot}, \end{aligned} \quad (2)$$

where  $[\text{Fe}/\text{H}]_s$  is the star's metallicity;  $Z_{\text{Fe}}$  and  $X$  are the iron and hydrogen mass fractions, respectively; and  $(Z/X)_{\odot}$  is the ratio for the solar mixture. We used  $(Z/X)_{\odot} = 0.0245$  ([Grevesse & Noels 1993](#)). This gives  $(Z/X) = 0.019 \pm 0.003$  for  $\beta$  Hvi.

From spectral analysis, [Dravins & Nordlund \(1990\)](#) found  $v \sin i = 2 \pm 1 \text{ km s}^{-1}$  for  $\beta$  Hvi. More recently, [Bruntt et al. \(2010\)](#) found  $v \sin i = 2.7 \pm 0.6 \text{ km s}^{-1}$ , and [Hekker & Aerts \(2010\)](#) from spectroscopic line-profile analysis, found  $v \sin i = 4.3 \text{ km s}^{-1}$ . From their analysis, [Hekker & Aerts \(2010\)](#) attempted to determine the inclination angle,  $i$ , of  $\beta$  Hvi, suggesting a value of  $55 \pm 17^\circ$  for this star. Thus the effect of rotation on the modelling of the structure of the star can be neglected. Similarly, since the resulting rotational splitting is comparable with the error in the observed frequencies (see below), in the present analysis we neglect the effects of rotation on the frequencies.

The position of  $\beta$  Hvi in the HR diagram is shown in Fig. 1 and the fundamental parameters we adopted are given in Table 1.

### 2.2. Seismic data

Asteroseismic observations of  $\beta$  Hvi have been reported by [Bedding et al. \(2007\)](#). They found an excess power centred around 1 mHz with a peak amplitude of  $\sim 50 \text{ cm s}^{-1}$ , and the oscillation frequencies show a comb-like structure typical of solar-like oscillations with a large frequency separation of the  $l = 0$  modes,  $\Delta\nu_0$ , of  $57.24 \pm 0.16 \mu\text{Hz}$ . They also identified 28 mode frequencies in the range  $0.7 < \nu < 1.4 \text{ mHz}$  with the angular degrees  $l = 0, 1, \text{ and } 2$ , three of which were identified as  $l = 1$  mixed modes. In this work, we used the updated list of 33 observed frequencies given in Table 2. To produce these, we reanalysed the 2005 dual-site observations ([Bedding et al. 2007](#)) using revised weights that were adjusted using a new method that minimises the sidelobes ([Kjeldsen et al., in prep.](#)). This method is described by [Bedding et al. \(2010\)](#), who applied it to multi-site observations of Procyon (see also [Arentoft et al. 2009](#)). In the same way as for Procyon, we extracted oscillation frequencies from the time series of  $\beta$  Hvi using the standard procedure of iterative sine-wave fitting. The finite mode lifetime causes many modes to be split into two or more peaks which, coupled with the presence of mode bumping, meant that deciding on a final list of mode frequencies with correct  $l$  identifications is somewhat subjective. We followed the same approach as [Bedding et al. \(2010\)](#), which involved using the ridge centroids as a guide and averaging multiple peaks into a single value. The remaining unidentified peaks in the power spectrum are listed in Table 3.

## 3. Modelling $\beta$ Hvi

### 3.1. Input physics to the models

To compute the evolutionary models we used the ‘‘Aarhus STellar Evolution Code’’, ASTEC ([Christensen-Dalsgaard 2008a](#)). The following assumptions were made: spherical symmetry, no rotation, no magnetic field and no mass loss. In the

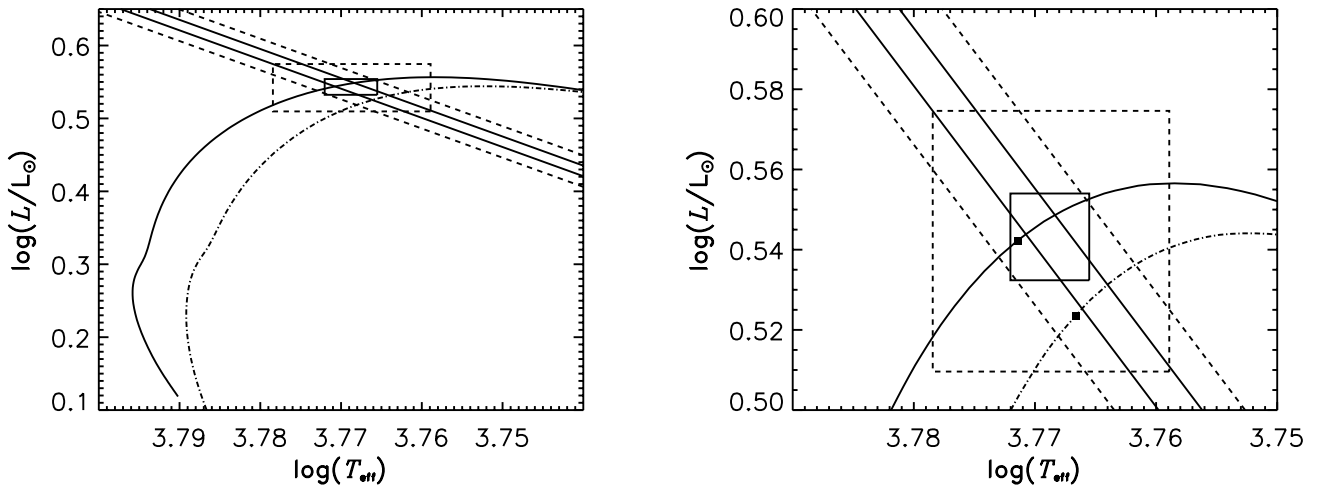


**Fig. 1.** *Left panel:* the position of  $\beta$  Hyi in the HR diagram. The constraints on the fundamental parameters ( $T_{\text{eff}}$ ,  $L/L_{\odot}$ ) are indicated by the 1- $\sigma$  error box (solid) and on the radius by diagonal solid lines. We also show the corresponding 3- $\sigma$  uncertainties by dashed lines. Two evolutionary tracks for the best models found by method 2 (cf. Table 5) are plotted with dash-dotted and solid curves, representing the models with and without gravitational settling and diffusion, respectively. *Right panel:* the same as in the left panel but zoomed in. The selected models are marked by filled squares.

**Table 1.** Stellar properties of  $\beta$  Hyi.

	Value	Reference
$\theta$ (mas)	$2.257 \pm 0.019$	North et al. (2007)
$\pi_p$ (mas)	$134.07 \pm 0.11$	van Leeuwen (2007)
$R/R_{\odot}$	$1.809 \pm 0.015$	Kjeldsen et al. (2008)
$L/L_{\odot}$	$3.494 \pm 0.087$	Current work
$T_{\text{eff}}$ (K)	$5872 \pm 44$	North et al. (2007)
[Fe/H]	$-0.10 \pm 0.07$	Bruntt et al. (2010)
Z/X	$0.019 \pm 0.003$	Current work

**Notes.** The luminosity,  $L$ , and radius,  $R$ , are expressed in solar units.  $\theta$  stands for the angular diameter,  $\pi_p$  for the *Hipparcos* parallax,  $T_{\text{eff}}$  for the effective temperature, [Fe/H] is the metallicity, and Z/X is the mass ratio of heavy elements to hydrogen.

computation we used the OPAL 2005 equation of state tables (see Rogers & Nayfonov 2002), OPAL opacities (Iglesias & Rogers 1996) complemented by low-temperature opacities from Ferguson et al. (2005), the solar mixture from Grevesse & Noels (1993), and the NACRE nuclear reaction rates (Angulo et al. 1999). We considered an atmospheric temperature versus optical depth relation which is a fit to the quiet-sun relation of Vernazza et al. (1976).

Convection was treated according to the standard mixing-length theory (MLT) from Böhm-Vitense (1958), where the characteristic length of turbulence,  $l_{\text{mix}}$ , scales directly with the local pressure scale height,  $H_p$ , as  $l_{\text{mix}} = \alpha H_p$ , leaving the scaling factor  $\alpha$  as a free parameter. MLT makes use of another free parameter associated with the amount of the core overshooting,  $\alpha_{\text{ov}}$ . Both Di Mauro et al. (2003) and Fernandes & Monteiro (2003) found that models at the position of  $\beta$  Hyi in the HR diagram are not affected by convective overshooting, so we decided, for this work, not to consider it in our models.

Diffusion and settling were treated in the approximations proposed by Michaud & Proffitt (1993). We refer to Christensen-Dalsgaard (2008a) for a detailed explanation.

**Table 2.** Observed oscillation frequencies in  $\beta$  Hyi (in  $\mu\text{Hz}$ ) resulting from the revised analysis, listed in ascending radial order within each column.

$l = 0$	$l = 1$	$l = 2$	$l = 3$
$660.74 \pm 2.43$	...	...	...
$716.68 \pm 3.00$	...	$711.24 \pm 2.13$	...
$774.79 \pm 2.20$	$802.74 \pm 1.69$	$769.97 \pm 0.99$	$791.66 \pm 1.35$
$831.86 \pm 2.43$	$857.32 \pm 0.86$	$825.86 \pm 1.18$	...
$889.15 \pm 1.23$	$912.91 \pm 0.86$	$883.35 \pm 0.89$	...
$946.11 \pm 0.91$	$959.98 \pm 0.89$	$939.97 \pm 0.97$	...
...	$987.08 \pm 0.87$	...	...
$1004.32 \pm 0.86$	$1032.99 \pm 0.86$	$999.40 \pm 0.91$	...
$1061.66 \pm 0.95$	$1089.87 \pm 0.88$	$1057.00 \pm 0.86$	...
$1118.67 \pm 0.88$	$1147.35 \pm 0.91$	$1115.20 \pm 1.06$	...
$1177.76 \pm 0.97$	$1203.54 \pm 1.01$	$1172.98 \pm 0.86$	$1198.16 \pm 1.23$
$1235.31 \pm 1.09$	...	...	...
...	$1320.42 \pm 0.94$	...	...
...	$1378.92 \pm 1.39$	...	...

**Notes.** The rows are in ascending  $l$ , and each row includes frequencies within  $\Delta\nu$ -sized-bits of the frequency spectrum. “...” is used for the modes whose S/N was too low for a clear extraction.

**Table 3.** Unidentified observed peaks with  $S/N \geq 3.5$ .

$\nu$ ( $\mu\text{Hz}$ )		
$753.12 \pm 1.57$	$1013.42 \pm 1.50$	$1130.36 \pm 1.30$
$828.70 \pm 1.83$	$1025.80 \pm 1.68$	$1134.32 \pm 1.63$
$845.02 \pm 1.61$	$1037.90 \pm 1.63$	$1167.62 \pm 1.10$
$868.60 \pm 1.13$	$1065.12 \pm 1.59$	$1256.78 \pm 1.60$
$911.88 \pm 1.76$	$1070.00 \pm 1.43$	$1383.20 \pm 1.75$
$1010.20 \pm 1.91$	$1084.20 \pm 1.57$	$1462.62 \pm 1.92$

### 3.2. Grids of models

We calculated two grids of evolutionary tracks, Grids I and II, with the input parameters shown in Table 4. In Grid II we included diffusion and gravitational settling of helium.

**Table 4.** Parameters used to compute the evolutionary tracks.

Parameter	Grid I	Grid II
$M/M_{\odot}$	1.00–1.18 (with steps of 0.02)	1.00–1.18 (with steps of 0.02)
$Z/X$	0.010–0.030 (with steps of 0.004)	0.010–0.030 (with steps of 0.004)
$Y$	0.24–0.30 (with steps of 0.02)	0.24–0.30 (with steps of 0.02)
Mixing length parameter ( $\alpha$ )	1.4–2.0 (with steps of 0.2)	1.4–2.0 (with steps of 0.2)
Diffusion & gravitational settling	None	He

**Notes.**  $M/M_{\odot}$  is the mass in solar units,  $Z/X$  is the initial ratio of heavy elements to hydrogen abundances, and  $Y$  the helium abundance.

For each grid, we took those models whose parameters were within the  $3\text{-}\sigma$  uncertainties derived from the observations of  $\beta$  Hyi, and computed the corresponding oscillation frequencies using the Aarhus adiabatic oscillation code ADIPLS (Christensen-Dalsgaard 2008b). The theoretical frequencies were then compared with the observed ones in order to find the best-matching model.

#### 4. Near-surface corrections

It is well known from helioseismology that there is a systematic offset between the observed and the computed oscillation frequencies of the Sun. This offset, which is nearly independent of the angular degree,  $l$ , of the mode and affects the highest frequencies the most (Christensen-Dalsgaard & Thompson 1997), arises from the improper modelling of the surface layers. Therefore, the offset is also expected to be present when comparing the observed and computed frequencies for other stars. Kjeldsen et al. (2008) used the solar data to derive an empirical correction for the near-surface offset, which can, in principle, be applied to other stars.

For the Sun, the difference between the observed,  $\nu_{\text{obs}}$ , and computed frequencies of the best model,  $\nu_{\text{best}}$ , was shown by Kjeldsen et al. (2008) to be well approximated by a power law fit given as

$$\nu_{\text{obs}}(n) - \nu_{\text{best}}(n) = a \left[ \frac{\nu_{\text{obs}}(n)}{\nu_0} \right]^b, \quad (3)$$

where  $n$  is the radial order, and  $\nu_0$  is a reference frequency that is chosen to be the frequency at maximum power. Since the offset is independent of  $l$ , the authors considered only radial ( $l = 0$ ) modes. Note that the ‘‘best model’’ is the one that best represents the interior but still fails to model the near-surface layers. They also argued that the frequencies of a reference model,  $\nu_{\text{ref}}$ , which is close to the best one, can be scaled from  $\nu_{\text{best}}$  by a factor  $r$ , i.e.,

$$\nu_{\text{best}}(n) = r\nu_{\text{ref}}(n). \quad (4)$$

Then Eq. (3) becomes

$$\nu_{\text{obs}}(n) - r\nu_{\text{ref}}(n) = a \left[ \frac{\nu_{\text{obs}}(n)}{\nu_0} \right]^b. \quad (5)$$

Kjeldsen et al. (2008), using the data and models for the Sun, found  $b = 4.90$ . Using this value for  $b$  it is possible to determine  $r$  and  $a$  from Eqs. (6) and (10) in Kjeldsen et al. (2008). Assuming that a similar offset occurs for other solar-like stars, they showed how to use the solar  $b$  to determine  $r$  and  $a$  from the observed frequencies of  $l = 0$  modes, and, consequently, use Eq. (5) to calculate the correction that must be applied to the frequencies computed for all  $l$  for a given stellar model. They noted that the correction applied to the mixed modes should be less than that for the pure  $p$  modes (see the next section).

#### 5. Selecting the best model

We considered two methods to find the model that to the closest extent possible reproduces the observed non-seismic and seismic data for  $\beta$  Hyi. For all models whose parameters were within the  $3\text{-}\sigma$  uncertainties derived from the non-seismic observations of  $\beta$  Hyi, we calculated the  $r$  and  $a$  values, following Kjeldsen et al. (2008), using  $b = 4.90$  and  $\nu_0 = 1000 \mu\text{Hz}$ .

In the first method we followed closely the work of Kjeldsen et al. (2008) and considered the best representative model to be the one having the value of  $r$  closest to 1, which means, from Eq. (4),

$$\nu_{\text{ref}}(n) \approx \nu_{\text{best}}(n). \quad (6)$$

Using the values of  $r$  and  $a$  found for this model, we then computed the correction factor to be applied to the model frequencies and compared them with those observed. Note, however, that in this method  $r$  is calculated using only the observed radial modes together with the corresponding model radial modes. If we assume that the best model is the one which has  $r$  closest to 1 then we are assuming the model that has the radial frequencies matching most closely the observed  $l = 0$  modes also has the nonradial frequencies matching best the observed  $l = 1$  and 2 modes, which may not be true.

In the second method we performed a statistical analysis, using the  $\chi^2$  test. Our goal was to find the reference model that, after applying the surface corrections, had the individual frequencies closest to the observed ones, for all  $l$ , i.e. we found the minimum of

$$\chi^2 = \frac{1}{N} \sum_{n,l} \left( \frac{\nu_{\text{ref,corr}}(n, l) - \nu_{\text{obs}}(n, l)}{\sigma(\nu_{\text{obs}}(n, l))} \right)^2, \quad (7)$$

where  $N$  is the total number of modes considered,  $\nu_{\text{ref,corr}}(n, l)$  are the frequencies of modes with radial order  $n$  and degree  $l$  of a reference model, corrected for the surface effects, and  $\sigma$  represents the uncertainty in the observed frequencies.

The correction term, as shown in the right-hand side of Eq. (3) can only be applied to the frequencies of the best model. In order to compute the correction term, since we have a set of reference models and we do not know which one is the best model, we assume that the corrected best  $\nu_{\text{best,corr}}$  and reference model  $\nu_{\text{ref,corr}}$  frequencies also scale as

$$\nu_{\text{best,corr}}(n, 0) = r\nu_{\text{ref,corr}}(n, 0). \quad (8)$$

We note that this is a good approximation because the surface corrections to the frequencies are much smaller than the frequencies themselves. Moreover, since  $\nu_{\text{best,corr}} \approx \nu_{\text{obs}}$  we have

$$\nu_{\text{ref,corr}}(n, 0) = \nu_{\text{ref}}(n, 0) + \left( \frac{a}{r} \right) \left[ \frac{\nu_{\text{obs}}(n, 0)}{\nu_0} \right]^b. \quad (9)$$

**Table 5.** The parameters of the best models found for Grid I (no diffusion) and II (He settling and diffusion), for each of the two methods.

Parameter	Grid I		Grid II	
	Method 1	Method 2	Method 1	Method 2
$M/M_{\odot}$	1.16	1.04	1.04	1.04
$R/R_{\odot}$	1.832	1.785	1.790	1.786
$L/L_{\odot}$	3.433	3.485	3.432	3.338
$T_{\text{eff}}$ (K)	5810	5908	5877	5843
Age (Gyr)	4.705	6.114	7.390	7.297
$Z$	0.0204	0.0124	0.0075	0.0075
$Y$	0.30	0.30	0.24	0.24
[Fe/H]	0.088	-0.133	-0.416	-0.424
$\alpha$	1.4	1.8	2.0	1.8
$r$	1.0000	0.9995	1.0000	1.0009
$a$ ( $\mu\text{Hz}$ )	-4.80	-3.14	-2.43	-3.11
$\Delta\nu_{0b}$ ( $\mu\text{Hz}$ )	58.977	58.488	58.243	58.400
$\Delta\nu_{0a}$ ( $\mu\text{Hz}$ )	57.678	57.652	57.600	57.577
$\chi^2$	19.086	1.183	26.226	2.642

**Notes.** The mass,  $M$ , luminosity,  $L$ , and radius,  $R$ , are expressed in solar units.  $T_{\text{eff}}$  is the effective temperature,  $Y$  and  $Z$  are the initial helium and heavy-element abundances, [Fe/H] is the metallicity at the surface, and  $\alpha$  is the mixing-length parameter. Also  $r$  and  $a$  are factors used to compute the correction term,  $\Delta\nu_{0b}$  and  $\Delta\nu_{0a}$  are, respectively, the large frequency separation before and after applying the surface correction to the model  $l = 0$  modes. The values of  $\chi^2$  are those calculated after correcting the frequencies for the near-surface effects.

Thus, Eq. (7) becomes

$$\chi^2 = \frac{1}{N} \sum_{n,l} \left( \frac{\nu_{\text{ref}}(n, l) + \left(\frac{a}{r}\right) \left[\frac{\nu_{\text{ref}}(n, l)}{\nu_0}\right]^b - \nu_{\text{obs}}(n, l)}{\sigma(\nu_{\text{obs}}(n, l))} \right)^2. \quad (10)$$

Note that, in practice, the term  $(a/r)[\nu_{\text{obs}}(n, 0)/\nu_0]^b$  on the right-hand side of Eq. (9) was replaced by  $(a/r)[\nu_{\text{ref}}(n, l)/\nu_0]^b$ . The reason is to enable us to correct all the reference model frequencies, instead of only the frequencies having the same radial order as those observed. The difference between these terms is minimal for the best-fitting model, and so we are safe in performing the replacement.

To compute  $\chi^2$  we used all the observed and computed  $l = 0, 1$ , and 2 frequencies. However, as already mentioned, some of the observed  $l = 1$  modes are mixed modes and the scaling is not valid for them. Mixed modes should not be affected by the surface layers as much as the p modes (Kjeldsen et al. 2008), so the correction term should be small for the mixed modes. Specifically, at a given frequency we expect the near-surface effects to scale inversely with the mode inertia, which is much higher for the mixed modes than for the p modes; thus we scaled the correction term by the inverse of the ratio  $Q_{nl}$  between the inertia of the mode and the inertia of a radial mode of the same frequency (Aerts et al. 2010). Taking that into account, Eq. (10) becomes

$$\chi^2 = \frac{1}{N} \sum_{n,l} \left( \frac{\nu_{\text{ref}}(n, l) + \left(\frac{1}{Q_{nl}}\right) \left(\frac{a}{r}\right) \left[\frac{\nu_{\text{ref}}(n, l)}{\nu_0}\right]^b - \nu_{\text{obs}}(n, l)}{\sigma(\nu_{\text{obs}}(n, l))} \right)^2. \quad (11)$$

In this method, our best model is the one that minimises Eq. (11).

Contrary to the first method, the  $\chi^2$  test takes into account all the individual frequencies, including mixed modes. This test also includes the uncertainties in the observations. Thus, it is possible that the model with the lowest  $\chi^2$  does not have the  $r$  that is closest to 1.

## 6. Results and discussion

The parameters of the best models found for Grids I and II, using the two methods described in Sect. 5, are shown in Table 5.

Figures 2 and 3 show the échelle diagrams for  $\beta$  Hyi. An échelle diagram shows the frequency spectrum divided into segments equally spaced by the large frequency separation, after these segments are stacked in the vertical direction (Grec et al. 1983). In these figures the observed frequencies of  $\beta$  Hyi are compared with the theoretical frequencies of the best models from Grid I (upper panel) and from Grid II (lower panel), both before (left plot) and after (right plot), applying the near-surface corrections. The model frequencies are represented by open symbols and the observed frequencies (cf. Table 2) by solid symbols, while the asterisks represent the unidentified peaks (cf. Table 3), which may correspond to genuine modes, sidelobes, or noise peaks. The relative sizes of the open symbols reflect the expected mode amplitudes (Christensen-Dalsgaard et al. 1995). The so-called mixed modes reveal themselves in the échelle diagrams, breaking the regularity of the ridges. The models predict mixed modes with all nonradial degrees, however mostly with too small amplitudes to be observed. On the other hand, some of the observed modes match well the mixed modes with  $l = 1$  (see, e.g., the right panels of Fig. 3). If we inspect Figs. 2 and 3, it is clear that the agreement between the observed and model frequencies is much better when method 2 is used (Fig. 3). This is due to the fact that in this method all the available seismic constraints were involved in selecting the best model.

It is seen from Table 5 that the model that has the  $r$  value closest to unity does not produce the lowest  $\chi^2$  value. The model with the lowest  $\chi^2$  still has an  $r$  satisfactorily close to unity. So, in addition to finding a model that represents the stellar interior reasonably, method 2 makes sure that all the available seismic constraints are simultaneously reproduced and so the fit, and hence the accuracy of the model, is improved substantially. This shows the importance of the individual modes in constraining the range of models to represent the observed star. Mixed modes, in particular, put strong constraints on the model properties, especially on the evolutionary stage. For instance, we can see from the right panels of Fig. 2 that two models resulting from method 1 have the two highest  $\chi^2$  values due to failing to match particularly the observed  $l = 1$  mixed modes. In the upper right panel, the model is too massive and it matches the rest of the seismic constraints before it is sufficiently evolved to have mixed modes, whereas

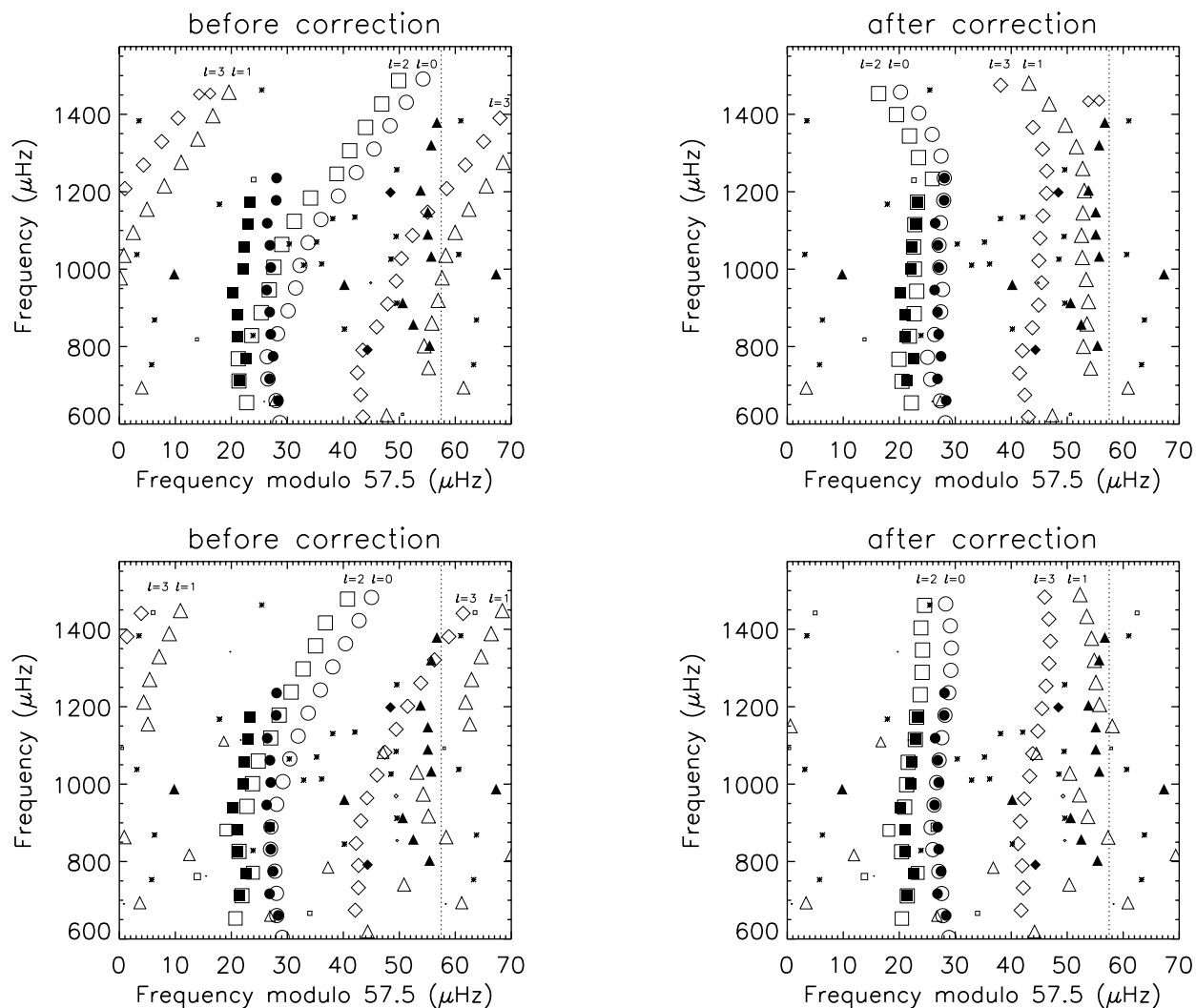


**Fig. 2.** Échelle diagrams for  $\beta$  Hyi, with a frequency separation of  $\Delta\nu = 57.5 \mu\text{Hz}$ , before (*left plot*) and after (*right plot*) application of the near-surface corrections to the model frequencies. Shown are the frequencies of the selected models using method 1, when including no diffusion (*upper panel*) and diffusion (*lower panel*). In method 1, the best model was selected using the radial ( $l = 0$ ) modes alone (see the text for details). The solid symbols show observed frequencies (Table 2), asterisks the unidentified peaks (Table 3), and the open symbols the model frequencies. Circles are used for  $l = 0$  modes, triangles for  $l = 1$ , squares for  $l = 2$  and diamonds for  $l = 3$ . Open symbols are scaled to represent the relative amplitudes of the modes as predicted by the models.

the model in the lower right panel does have mixed modes, although the predicted mixed modes do not match those observed.

In general, we found that the empirical surface corrections proposed by Kjeldsen et al. (2008) work very well for  $\beta$  Hyi as seen from Figs. 2 and 3, although there is room for improvement for high-frequency modes of  $l = 1$ . The reason for the suboptimal agreement for those modes is that the correction term is determined using only the  $l = 0$  observed modes, whose frequencies span a smaller range than those of the  $l = 1$  modes. Thus, radial modes with higher frequencies need to be detected in order to improve the agreement for the higher frequency  $l = 1$  modes. Note that the change in the large frequency separation of the models after applying the near-surface correction is around  $0.8 \mu\text{Hz}$ , which is larger than the given uncertainty of the observed large separation. This should be taken into account when modelling through a pipeline analysis that uses the large separation as input. It is encouraging to see that we can observe  $l = 3$  modes, and that some of the unidentified modes are also

close to the model frequencies, namely  $753.1 \mu\text{Hz}$  ( $l = 1$ ?) and  $1462.6 \mu\text{Hz}$  ( $l = 0$ ?).

Even though the best model seems to be the one without diffusion, we do expect that within a star diffusion occurs. The two selected models, the ones with and without diffusion, resulting from the method 2 are in fact compatible and both could be further fine-tuned.

## 7. Summary and conclusions

We computed two grids of evolutionary models, using the ASTEC code, in order to find the model that most closely reproduces the seismic and non-seismic data of  $\beta$  Hyi. The parameters used for each grid are given in Table 1. We computed the oscillation frequencies for the models that lie inside the  $3\text{-}\sigma$  error box of the star's position in the HR diagram with the ADIPLS code, and compared them with the observed frequencies. There is an offset needed to be taken into account in this comparison, due to improper modelling of the near-surface lay-

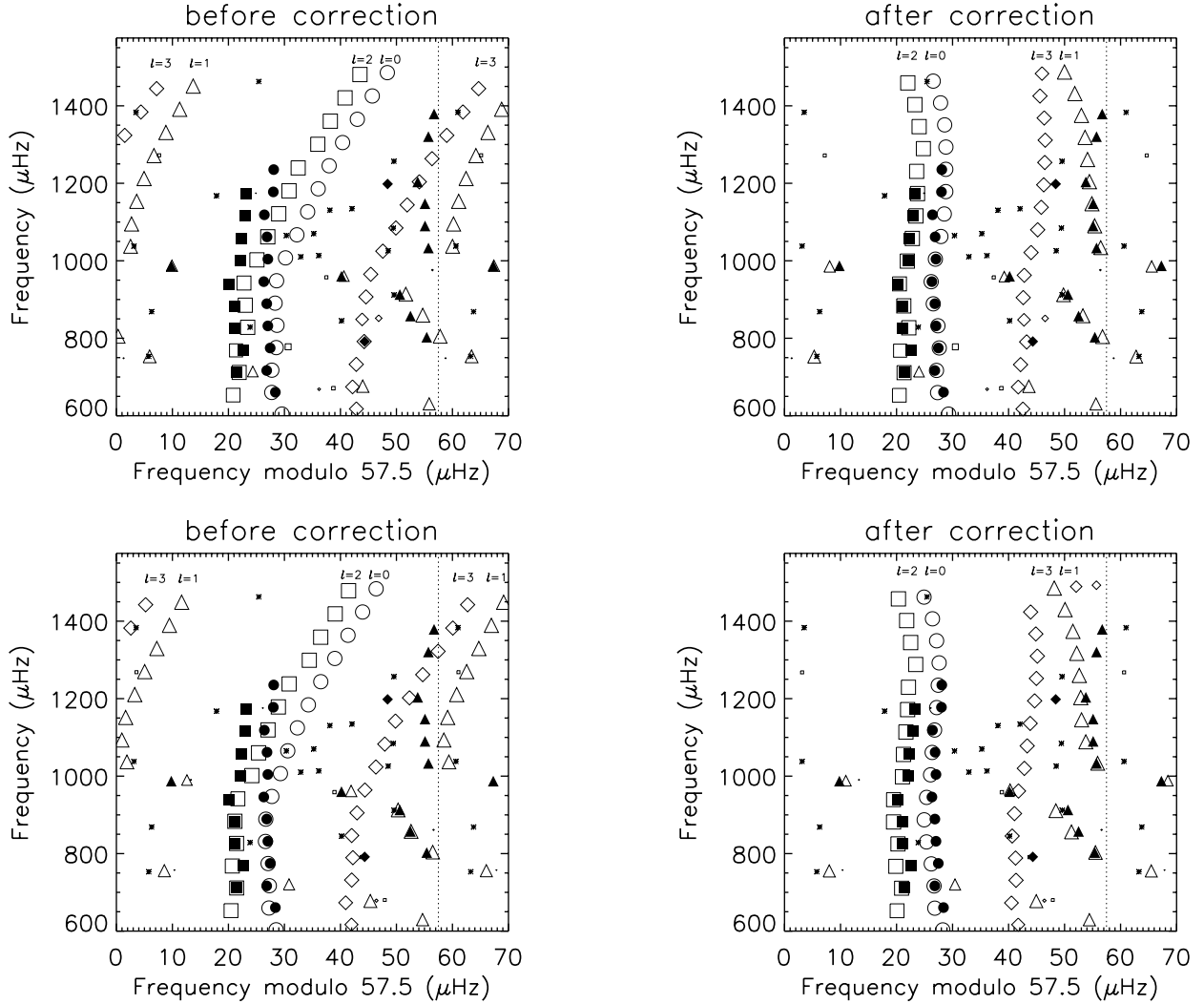


**Fig. 3.** The same as Fig. 2 but for the best models without (*upper panel*) and with (*lower panel*) diffusion, selected using method 2, which takes into account the observed and identified modes with all degrees available.

ers of the stars. We used the approach proposed by Kjeldsen et al. (2008) to correct the computed frequencies of  $\beta$  Hyi from this offset. We used two methods in order to find the model that reproduces the observed oscillation frequencies of  $\beta$  Hyi.

In our analysis, we argue that the method involving the  $\chi^2$  test, method 2, is the most robust way to find the best model, since it takes into account all the individual frequencies, the mixed modes, and also the uncertainties on the observed frequencies. Analysing the échelle diagrams of the representative models found with method 2 (cf. Sect. 6), we see that the surface correction works very well for  $l = 0$  modes, and for  $l = 1$  and 2 modes with frequencies lying in the frequency range of the observed radial modes. This was expected since the correction term was computed using only those radial modes. Observed  $l = 0$  modes with higher frequencies are thus needed in order to improve the surface correction.

Our best models give  $M = 1.04 M_{\odot}$  and an age of 6.1–7.3 Gyr for  $\beta$  Hyi, depending on the inclusion of gravitational settling and diffusion of helium. In either case, the radius is found to be  $R \sim 1.785 R_{\odot}$ , which is in good agreement with the one determined by interferometry,  $R = 1.809 \pm 0.015 R_{\odot}$ . However, there are other models fitting the data similarly well. We used the parameters of those models (with  $\chi^2 < 10$ ) to de-

termine the internal error regarding our analysis. We calculated the mean value, and the uncertainties were taken as the standard deviation. We found  $M = 1.08 \pm 0.03 M_{\odot}$ , age =  $6.40 \pm 0.56$  Gyr, and  $R = 1.811 \pm 0.020 R_{\odot}$ . These results are also consistent with the results of Fernandes & Monteiro (2003), who derived,  $M = 1.10^{+0.04}_{-0.07} M_{\odot}$  and  $M = 1.09 \pm 0.22 M_{\odot}$ , through the HR diagram analysis and  $\Delta\nu_0$ , respectively, and a stellar age between 6.4 and 7.1 Gyr.

*Acknowledgements.* This work was partially supported by the project PTDC/CTE-AST/098754/2008 and the grant SFRH/BD/41213/2007 funded by FCT / MCTES, Portugal. M.C. is supported by a Ciência 2007 contract, funded by FCT/MCTES (Portugal) and POPH/FSE (EC). G.D., J.C.D., and H.K. are grateful for the financial support from the Danish Natural Science Research Council. TRB is supported by Australian Research Council. NCAR is supported by the U.S. National Science Foundation.

## References

- Aerts, C., Christensen-Dalsgaard, J., & Kurtz, D. W. 2010, *Asteroseismol.* (Heidelberg: Springer)
- Aizenman, M., Smeyers, P., & Weigert, A. 1977, *A&A*, 58, 41
- Angulo, C., Arnould, M., Rayet, M., et al. 1999, *Nucl. Phys. A*, 656, 3
- Arentoft, T., Kjeldsen, H., & Bedding, T. R. 2009, *ASP Conf. Ser.* 416, ed. M. Dikpati, T. Arentoft, I. González Hernández, C. Lindsey, & F. Hill, 347
- Bahcall, J. N., Pinsonneault, M. H., & Basu, S. 2001, *ApJ*, 555, 990

- Bedding, T. R., Butler, R. P., Kjeldsen, H., et al. 2001, *ApJ*, 549, L105
- Bedding, T. R., Kjeldsen, H., Arentoft, T., et al. 2007, *ApJ*, 663, 1315
- Bedding, T. R., Kjeldsen, H., Campante, T. L., et al. 2010, *ApJ*, 713, 935
- Biazzo, K., Pasquini, L., Girardi, L., et al. 2007, *A&A*, 475, 981
- Blackwell, D. E., & Lynas-Gray, A. E. 1998, *A&AS*, 129, 505
- Böhm-Vitense, E. 1958, *Z. Astrophys.*, 46, 108
- Bruntt, H., Bedding, T. R., Quirion, P., et al. 2010, *MNRAS*, 746
- Carrier, F., Bouchy, F., Kienzle, F., et al. 2001, *A&A*, 378, 142
- Christensen-Dalsgaard, J. 2008a, *Ap&SS*, 316, 13
- Christensen-Dalsgaard, J. 2008b, *Ap&SS*, 316, 113
- Christensen-Dalsgaard, J., & Thompson, M. J. 1997, *MNRAS*, 284, 527
- Christensen-Dalsgaard, J., Bedding, T. R., & Kjeldsen, H. 1995, *ApJ*, 443, L29
- Cunha, M. S., Aerts, C., Christensen-Dalsgaard, J., et al. 2007, *A&AR*, 14, 217
- da Silva, L., Girardi, L., Pasquini, L., et al. 2006, *A&A*, 458, 609
- di Benedetto, G. P. 1998, *A&A*, 339, 858
- Di Mauro, M. P., Christensen-Dalsgaard, J., & Paternò, L. 2003, *Ap&SS*, 284, 229
- Doğan, G., Brandão, I. M., Bedding, T. R., et al. 2009, *Ap&SS*, 251
- Dravins, D., & Nordlund, A. 1990, *A&A*, 228, 203
- Dravins, D., Linde, P., Ayres, T. R., et al. 1993a, *ApJ*, 403, 412
- Dravins, D., Linde, P., Fredga, K., & Gahm, G. F. 1993b, *ApJ*, 403, 396
- Dravins, D., Lindegren, L., Nordlund, A., & Vandenberg, D. A. 1993c, *ApJ*, 403, 385
- Edmonds, P. D., & Cram, L. E. 1995, *MNRAS*, 276, 1295
- Evans, D. S., Menzies, A., & Stoy, R. H. 1957, *MNRAS*, 117, 534
- Favata, F., Micela, G., & Sciortino, S. 1997, *A&A*, 323, 809
- Ferguson, J. W., Alexander, D. R., Allard, F., et al. 2005, *ApJ*, 623, 585
- Fernandes, J., & Monteiro, M. J. P. F. G. 2003, *A&A*, 399, 243
- Frandsen, S. 1987, *A&A*, 181, 289
- Gray, R. O., Corbally, C. J., Garrison, R. F., et al. 2006, *AJ*, 132, 161
- Grec, G., Fossat, E., & Pomerantz, M. A. 1983, *Sol. Phys.*, 82, 55
- Grevesse, N., & Noels, A. 1993, in *Origin and Evolution of the Elements*, ed. S. Kubono, & T. Kajino, 14
- Hekker, S., & Aerts, C. 2010, *A&A*, 515, A43
- Hoffleit, D., & Warren, J. W. H. 1995, *VizieR Online Data Catalog: V/50, SIMBAD*
- Iglesias, C. A., & Rogers, F. J. 1996, *ApJ*, 464, 943
- Kjeldsen, H., Bedding, T. R., & Christensen-Dalsgaard, J. 2008, *ApJ*, 683, L175
- Michaud, G., & Proffitt, C. R. 1993, in *Inside the Stars*, ed. W. W. Weiss, & A. Baglin, IAU Coll., 137, ASP Conf. Ser., 40, 246
- North, J. R., Davis, J., Bedding, T. R., et al. 2007, *MNRAS*, 380, L80
- Osaki, J. 1975, *PASJ*, 27, 237
- Perryman, M. A. C., & ESA 1997, *The HIPPARCOS and TYCHO catalogues. Astrometric and photometric star catalogues derived from the ESA HIPPARCOS Space Astrometry Mission, ESA SP, 1200*
- Rogers, F. J., & Nayfonov, A. 2002, *ApJ*, 576, 1064
- Santos, N. C., Israelian, G., Mayor, M., et al. 2005, *A&A*, 437, 1127
- van Leeuwen, F. 2007, *A&A*, 474, 653
- Vernazza, J. E., Avrett, E. H., & Loeser, R. 1976, *ApJS*, 30, 1
- Wheeler, J. C., Snedden, C., & Truran, J. J. W. 1989, *ARA&A*, 27, 279